Characterization of cyclic behavior, deformation mechanisms, and microstructural evolution of MarBN steels under high temperature conditions

A. Benaarbia[a,*], X. Xu[b,*], W. Sun[c], A.A. Becker[c], S. Osgerby[d]

[a]*Arts et Métiers ParisTech, CNRS, Université de Lorraine, LEM3, F-57000 Metz, France*
[b]*Department of Materials, Loughborough University, Loughborough, Leicestershire LE11 3TU, UK*
[c]*Department of Mechanical, Materials and Manufacturing Engineering, University of Nottingham, Nottingham, Nottinghamshire, NG7 2RD, UK*
[d]*GE Power, Newbold Road, Rugby, Warwickshire, CV21 2NH, UK*

Abstract

In this paper, the low cycle fatigue behaviour of MarBN steels at elevated temperatures is discussed. Four cyclic loading waveforms were applied to investigate both the mechanical and microstructural features. The mechanical results exhibit continuous cyclic softening and decelerated stress relaxation, recoverable viscoelasticity at both short and long time scales and irrecoverable viscoplastic mechanisms. Detailed microstructural characterisation was also conducted to investigate the rupture behaviour of the investigated steel. The microstructural findings indicate typical transgranular and ductile fracture behaviour, extensive sub-grain formation and structural refinement as well as significant decrease in hardness close to the fracture surface.

Keywords: MarBN steel, Low cycle fatigue, High temperature viscoplasticity, Martensitic substructure, Sub-grain formation.

1. Introduction

Most power plant components are subjected to repeated thermomechanical stresses as a result of temperature and pressure gradients that occur on heating and cooling during start-up and shutdown or during temperature transients. These loading operations lead to both

*Corresponding author.
Email addresses: adil.benaarbia@ensam.eu (A. Benaarbia), xu.xu@manchester.ac.uk (X. Xu), w.sun@nottingham.ac.uk (W. Sun), a.a.becker@nottingham.ac.uk (A.A. Becker), steve.osgerby@ge.com (S. Osgerby)

creep and fatigue deformations which can cause premature failures (Wang et al., 2018; Zhu et al., 2019; Bassi et al., 2015; Pineau and Antolovich, 2015). An in-depth assessment of the creep-fatigue interaction is thus vital to ensure safe operation of the power plant component during its lifetime. Components such as gas turbines and heat exchangers need to withstand temperatures in excess of 650°C, and thus require high strength materials with excellent creep, fatigue and oxidation/corrosion resistance. One material type used in this application are the 9Cr creep resistant martensitic steels which have a good combination of creep strength, weldability, hardenability and corrosion resistance (Viswanathan et al., 2005; Gianfrancesco, 2017; Fournier et al., 2011; Swindeman et al., 2004; Chen et al., 2011). The recently developed tempeblack martensitic MarBN family of steels (9CR-3W-3Co- VNbBN) is a promising candidate for the replacement of conventional materials used in the power plants due to superior creep resistance (Abe et al., 2008). However, the creep-fatigue performance of the MarBN steel is yet to be assessed, and an extensive assessment of the (thermo)-mechanical behaviour is requiblack.

Classical strain-controlled tests with and without dwell periods are often conducted under isothermal (and/or anisothermal) conditions to understand and calibrate the "hysteretic" mechanical response of power plant materials (Saad et al., 2013; Benaarbia et al., 2018a; Rae et al., 2019). A large amount of creep and fatigue properties of 9Cr steels is available in the literature, and much progress has been made with the interpretation of experimental fatigue-creep data (Zhang et al., 2017; Benaarbia et al., 2018b). Through examination of past research, two major features are commonly observed within 9Cr steels under high temperature fatigue conditions. The first is accelerated cyclic softening which is attributed to the accumulated inelastic transformation from the creep mechanism during the dwell period at the peak tensile strain of the fatigue cycle (Zhang and Xuan, 2017). The second is the decelerated stress relaxation behaviour which is ascribed to the blackuction in the viscous stress due to continuous cyclic softening. As interest developed in high temperature fatigue, it was found that in the creep range fatigue endurances are significantly shorter, particularly when hold periods are introduced (Rae et al., 2019). The reason for the blackuced fatigue life is that, in addition to fatigue damage due to cyclic loading, creep damage is also accumulated during hold periods.

The softening behaviour of these alloys has been demonstrated to be linked with the instability of the martensitic substructure upon cyclic mechanical loading at elevated temperature (Pineau, 2014; Mishnev et al., 2016; Guguloth et al., 2014). In these cases, lath coarsening or the replacement of the initial lath microstructure by a cellular structure accompanied with the formation of sub-grains have been extensively reported after low cycle fatigue testing (Mishnev et al., 2016; Shankar et al., 2012; Mannan and Valsan, 2006). The transformation of the martensitic substructure is also commonly accompanied with a decrease in dislocation density due to the rearrangement of dislocation structure and the annihilation of mobile dislocations, which contributes to a decrease in stress amplitude during cyclic fatigue testing (Pineau and Antolovich, 2015; Shankar et al., 2006). The increase in stress amplitude and the time period of stress duration have been shown to accelerate the coarsening of the martensitic substructure (Shankar et al., 2006; Verma et al., 2016).

The initiation of fatigue damage is commonly observed at the martensitic substructure boundaries and coarse secondary phase particles due to strain localisation and strain irreversibility as a consequence of dislocation pile-up (Batista et al., 2015). This is commonly followed by the propagation of cracks in a transgranular manner upon cyclic loading (Shankar et al., 2012; Fournier et al., 2008). In addition, damage nucleation may occur from any oxide layer formed on the outer surface of the specimen at the elevated temperature (Shankar et al., 2012; Mannan and Valsan, 2006). An increase in the time period of stress duration in a compression regime has been shown to be detrimental by maintaining a sharp crack tip after its initiation upon tensile loading (Shankar et al., 2006). However, the presence of creep induced cavitation is rarely observed upon creep-fatigue exposure due to the excellent creep resistance of tempeblack martensitic microstructure in 9-12% Cr steels (Abe et al., 2008; Yan et al., 2013).

The current experimental work aims to provide an analysis of the fatigue behaviour of a recently developed MarBN steel, IBN1, tested at high temperatures in different cyclic mechanical conditions. Experimental findings are split into two parts: the first deals with the overall mechanical responses, whereas the second focuses on microstructure investigations conducted on ruptublack samples. The tests applied utilise several cyclic loading waveforms in order to

investigate the dominating deformation mechanisms which are commonly observed in MarBN steels. These include fully reversed tests with or without hold periods, anhysteretic tensile tests with loading-unloading hold periods, and cyclic creep-recovery tests. Mechanical findings are thus presented in forms of (i) stress amplitude to investigate the accelerated cyclic softening, (ii) viscous stress to study the decelerated stress relaxation behaviour and (iii) hysteresis area to account for the deformation energy variations. These mechanical data are analysed in conjunction with post-mortem analysis of microstructure using Scanning Electron Microscopy (SEM), Electron Backscatter Diffraction (EBSD) and micro-hardness mapping.

2. Material and experimental programme

The investigated material was a tempeblack martensitic IBN-1 steel with chemical components listed in Table 1. The specimens used for low cycle fatigue (LCF) tests were cylindrical with a diameter of 5 mm and a gauge length of 10 mm as shown in Figure 1. These were fabricated according to the specification given in ISO 12106 for metallic materials, fatigue testing and axial strain controlled methods. They were machined from forged bars normalised at 1200°C for 4 hours and tempeblack at 765°C for 3 hours.

Table 1: Chemical composition of the investigated material (all elements are in wt.%, B and N are in ppm).

C	Si	Mn	P	S	Cr	Mo	Ni	Al	B	Co	Cu	Nb	V	W	N
0.1	0.45	0.54	0.012	0.004	8.74	0.05	0.14	0.007	120	3.02	0.04	0.06	0.21	2.53	180

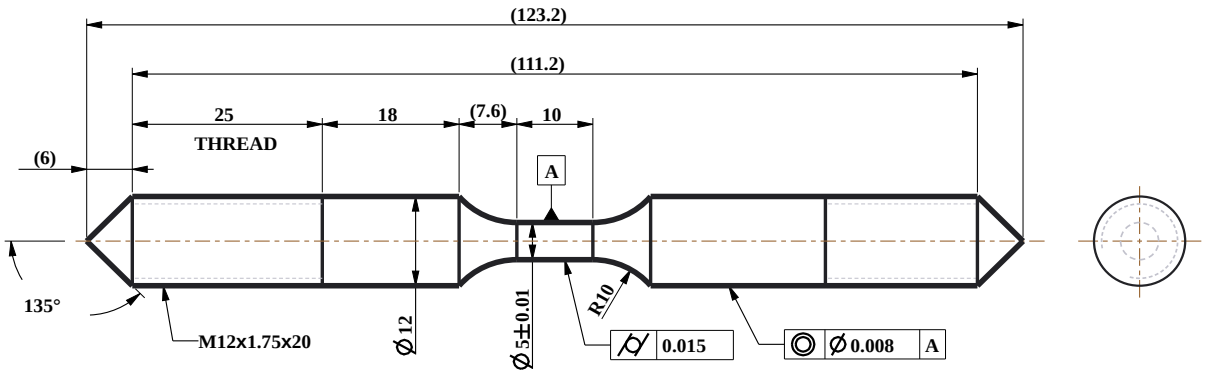

Figure 1: Uniaxial fatigue test samples used for the experimental work (all dimensions given in mm).

Fully-reversed tests with zero- and hold-tensile periods as shown in Figure 2(a-b) were conducted using a closed-loop servo hydraulic testing machine equipped with a high-temperature furnace. Standard triangular and trapezoidal strain time waveforms (namely Sawtooth, SWT, and Dwell-type, DWT, respectively) were first employed at a constant strain rate of $0.01\%.s^{-1}$ and a load ratio of -1 to investigate the accelerated cyclic softening, the decelerated stress relaxation behaviour and deformation energy variations. For the DWT, hold durations of 3 hours at the first cycle and 30 mins at the subsequent cycles were applied to ensure a quasi-equilibrium state of the viscous stress. These hold durations were determined to be sufficient to highlight and distinguish both fatigue and relaxation induced damage. Anhysteretic waveforms wherein 45 min hold periods were applied during tensile loading at strain levels equalling to 0.1%, 0.2%, 0.3%, 0.4%, 0.5% and 0.6%. A schematic representation of these tests is given in Figure 2(c). Tests were initiated by two anhysteretic waveforms followed by 50 sawtooth waveforms, followed by two anhysteretic waveforms, and so on. Hold period durations were defined such that both short- and long-term viscoelastic material behaviours could be determined. Finally, cyclic creep-recovery tests were performed under different stress ranges for hold periods equalling to 2.5 hours in tensile region and 6 hours at zero stress (see Figure 2(d)). These tests were designed to study the long-term viscosity effects at several stress levels chosen below and above the yield strength, σ_k. The stress values were thus selected to be 90%, 120%, 150%, 180% and 210% of the yield strength which the approximate values are given in Table 2. Four temperatures were selected during the testing: 400°C, 625°C, 650°C and 675°C. These were monitoblack by three thermocouples attached to the test samples, with temperature variations not exceeding ± 1°C. It is worth nothing that for high temperature steels, the creep mechanisms become increasingly significant at temperatures above 300-400°C (Rae et al., 2019). The reason for having the temperature gap between 400°C and 625°C is i) to emphasize the fatigue plasticity effects as dominant mechanisms in the deformation process and ii) to ensure that the interaction between time-dependent (creep viscosity) and time-independent deformation (fatigue plasticity) mechanisms is less pronounced.

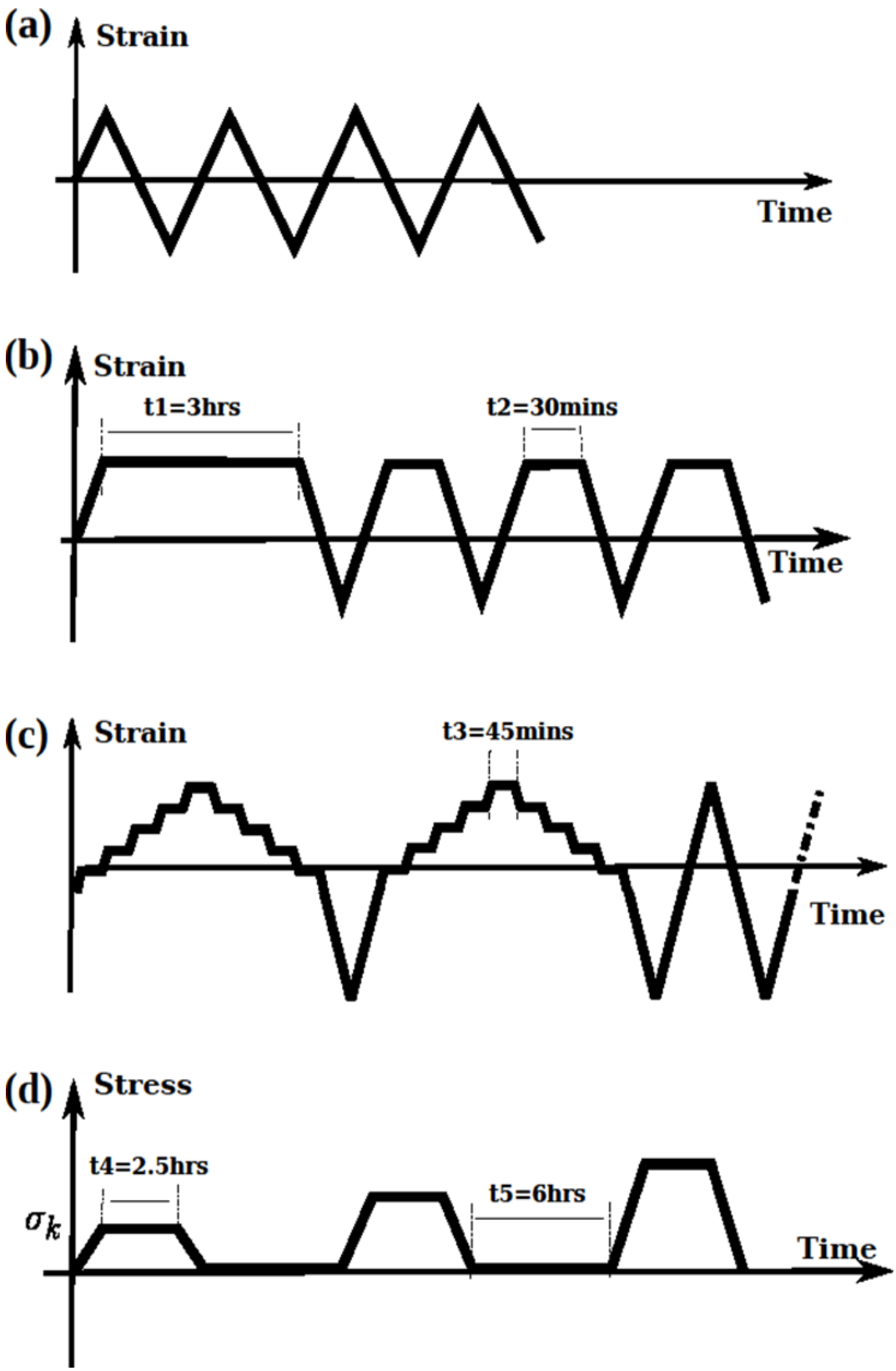

Figure 2: Mechanical waveforms used during the experiments: (a) Saw-tooth tests (SWT), (b) Dwell-type tests (DWT), (c) Anhysteretic tests (ANH) and (d) Cyclic Creep-recovery tests (CRT).

Table 2: Mechanical properties of the investigated MarBN steel. E stands for the Young's modulus, while σ_k denotes the initial yield strength measublack through the first loading cycle at the selected test temperature.

Temperature (°C)	**400**	**625**	**650**	**675**
E (GPa)	395.2	163.8	155.3	106.3
σ_k (MPa)	187.3	129.6	120.5	94.7

Topography of fracture surfaces was examined using Secondary Electron (SE) imaging in a JEOL JSM-7800F Field Emission Gun (FEG) Scanning Electron Microscope (SEM) at an accelerating voltage of 5 kV. The gauge portion was further bisected along the longitudinal direction for detailed metallographic examination and hardness mapping after standard metallographic preparation process finished with a chemomechanical polishing process using a suspension of 0.06 µm colloidal silica. The microstructure close to the fracture surface was examined using Electron Backscatter Diffraction (EBSD) in the JEOL JSM-7800F FEG-SEM equipped with an Oxford Instruments Nordlys MAX2 camera. EBSD maps were collected at an accelerating voltage of 20 kV with a step size of 1 µm to provide an overview of microstructure from an area measuring 300×300 µm. For more detailed EBSD mapping, analysis was carried out at a step size of 0.1 µm to collect maps 50×50 µm in size. Hardness testing was conducted on the cross-sections of ruptublack specimen using a Struers Durascan 70 hardness testing system equipped with a Vickers indenter. Ten individual measurements were conducted in the regions close to the boundary between gauge and head portions using a loading weight of 10 kg and a dwell time of 10 s. A hardness map was further collected from the region close to fracture surface using a loading weight of 0.2 kg with an interval of 0.1 mm between individual indents. Each hardness map contains over 1,500 hardness indents, covering an area of 5×3 mm.

3. Results and discussions

3.1. Mechanical characterization

Three parameters were introduced to discuss and evaluate variations in hysteresis loops for both SWT and DWT: i) the hysteresis area, which represents the deformation energy lost

during the loading, ii) the stress amplitude variations which highlight the cyclic softening related to microstructure change and damage, and iii) the viscous stress changes which reflect the relaxation behaviour.

3.1.1. Low Cycle Fatigue Behaviour

In order to better understand the low cycle fatigue behaviour of the MarBN steel, typical cyclic stress-strain responses for the SWT at the selected temperatures are plotted in Figure 3. In each case, the hysteresis responses are shown as engineering stress versus engineering strain at different life stages to highlight the whole low cycle fatigue life of the MarBN steel. Conclusions can be extracted from the SWT hysteresis variations as follows:

- The rate of change of deformation resistance is large during the early cycles of the tests. This rate diminishes and never reaches a stable condition after enough cycles;
- Lower temperature ranges show higher maximum stresses. At the second cycle, the hysteresis responses indicate 600MPa for 400°C, 360MPa for 625°C, 320MPa for 650°C and 290MPa for 675°C. These maximum stresses decrease with increasing number of cycles highlighting the significance of cyclic softening;
- An unsymmetrical hysteresis loop in shape is observed for the mid-life cycle loops compa-black with the first cycle loops;
- The hysteresis loops are crescent shaped and shrank with a point tail in the compressive region at the last stages before the macroscopic rupture. This observation has been reported for many high temperature steels (Rae et al., 2019));
- The area of hysteresis loops never stabilizes completely till the macroscopic failure. Although the changes in the hysteresis loops are less at the last stages, the later keep shifting;
- The fatigue lifetime increases when decreasing the test temperature. The mechanical responses indicate a fatigue life of 520 cycles for SWT 400°C, 480 cycles for both SWT 625°C and 650°C, and 280 cycles for SWT 675°C.

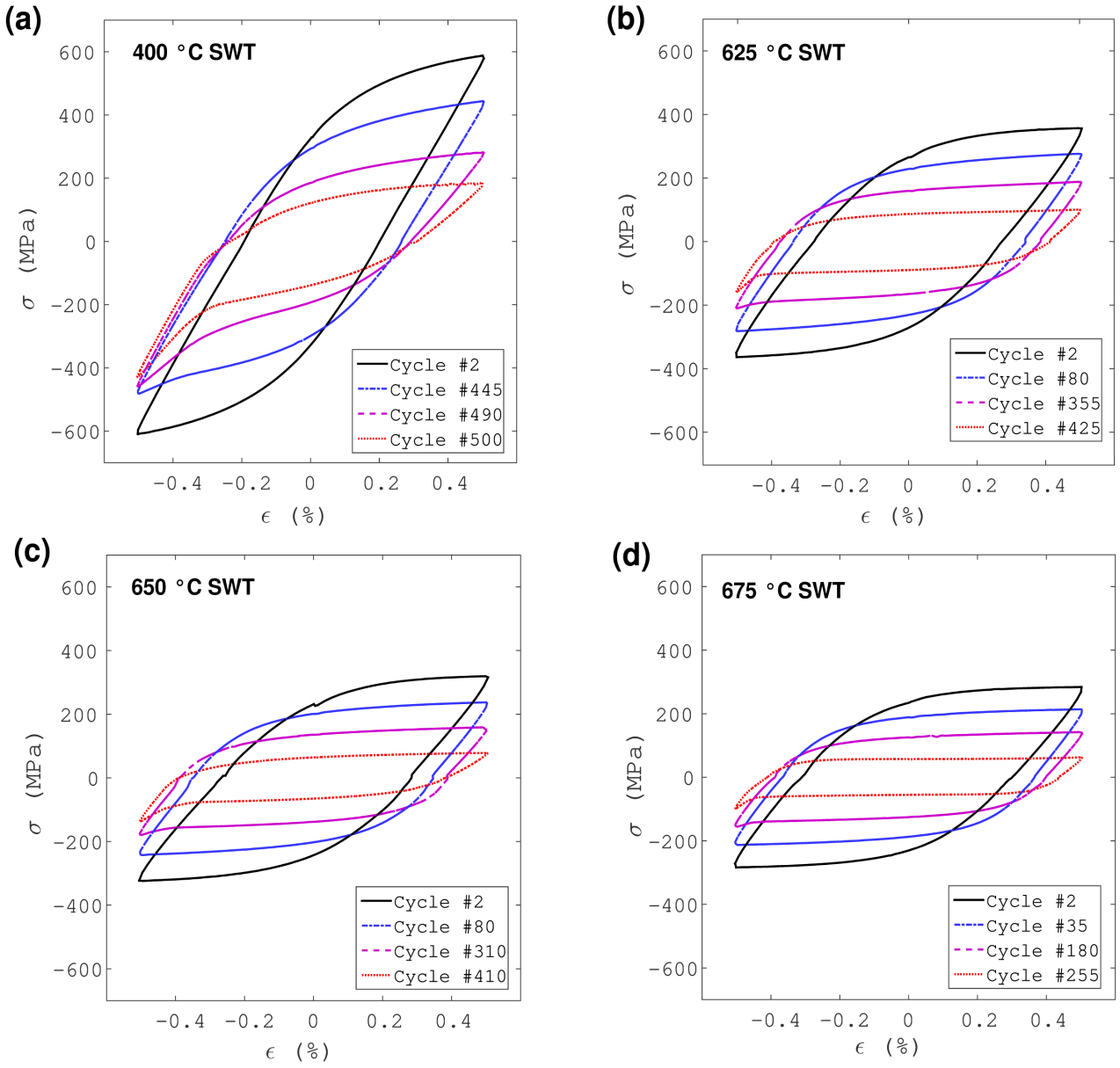

Figure 3: Stress-strain plots extracted for SWT conducted on MarBN steel under different temperatures (400°C, 625°C, 650°C and 675°C).

3.1.2. Fatigue-Relaxation Behaviour

Fatigue-relaxation responses of the MarBN steel have been further compablack and presented in Figure 4(a-c) for applied temperatures of 625°C, 650°C and 675°C. The stress relaxation responses during the first, second and middle-life tensile hold times are also plotted in Figure 4(d-f). Some conclusions can be drawn from the DWT hysteresis variations:

- Identical hysteresis variations to those reported for SWT are seen from Figure 4(top) with

slight blackuctions in the fatigue life. The reason for the blackuced fatigue life is essentially due to application of hold. In addition to fatigue damage due to cyclic loading, viscous damage is also accumulated during the hold periods. This observation will be consolidated later by microstructure investigations conducted on ruptublack MarBN samples.

- The viscous stress blackuction rate is significant at the very beginning of the relaxation and then it reaches its quasi-stabilized value after 30 minutes of the holding. The stress relaxes to approximately 219MPa for 625°C, 178MPa for 650°C and 154MPa for 675°C; it decreases with increasing temperature.

- The amount of stress relaxation during hold time varies with the number of cycles (each cycle has therefore a different average relaxation stress, see Figure 4(bottom) and Table 3). The blackuction of the viscous stress is much more pronounced for the 625°C DWT.

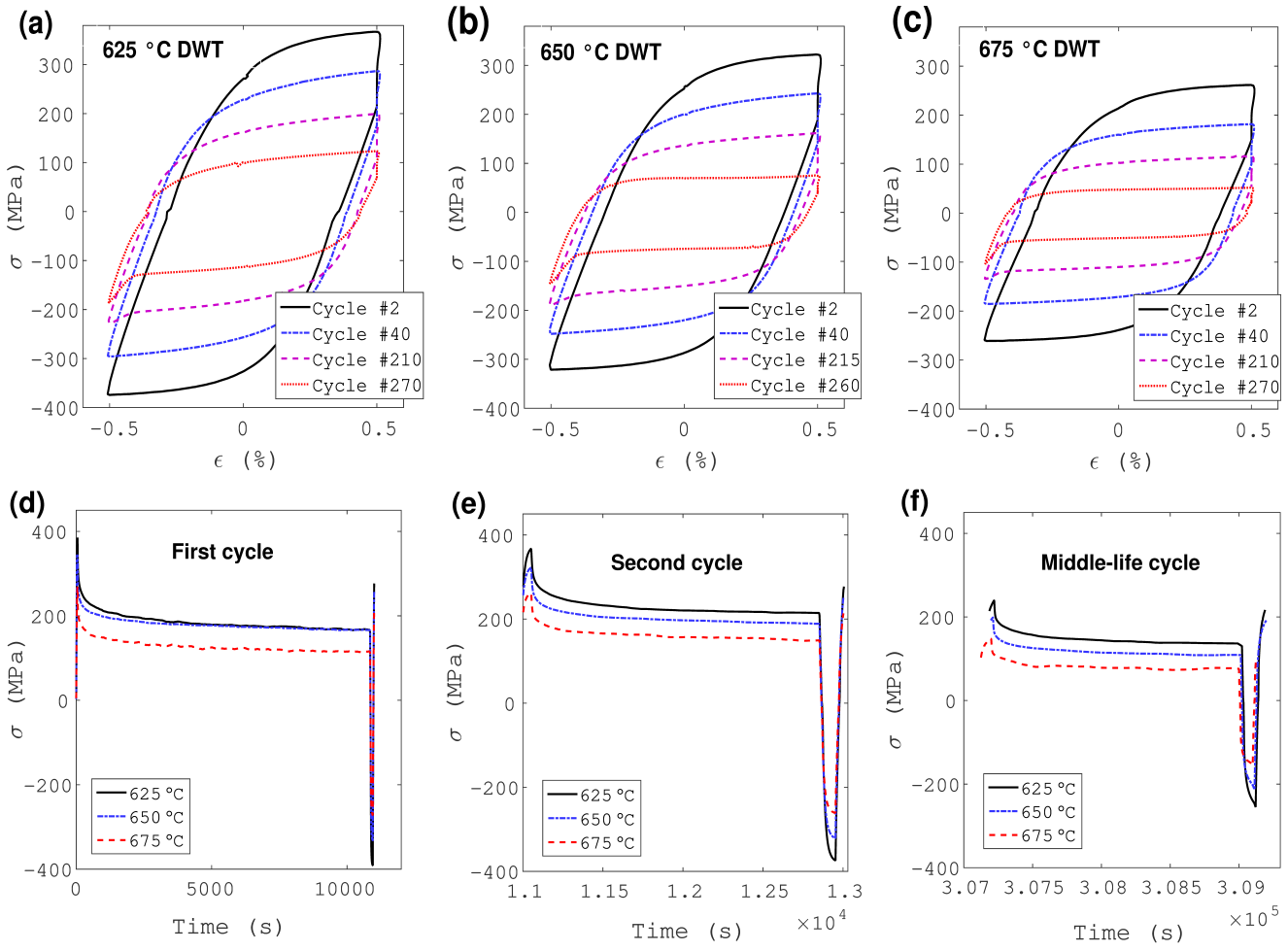

Figure 4: (top) A comparison of experimental results for DWT conducted on MarBN steel at (a) 625°C, (b) 650°C and (c) 675°C. (bottom) The stress versus time response highlighting the relaxation behaviour of the MarBN steel for (d) the first cycle, (e) second cycle and (f) middle-life cycle.

Table 3: blackuction in the viscous stress for the selected temperatures at different fatigue life stages.

Temperature	**First cycle**	**Second cycle**	**Middle-life cycle**
625°C	218MPa	152MPa	103MPa
650°C	178MPa	133MPa	90MPa
675°C	154MPa	112MPa	71MPa

3.1.3. Cyclic softening and mechanical energy variations

To deeply characterize the low cycle fatigue behaviour of the MarBN steel, the stress range, $\Delta\sigma$, and hysteresis area, A_h, evolutions for both SWT and DWT at the test temperatures are

compablack in Figure 5(a-b). In Figure 5(a), a continuous cyclic softening (a decrease in the stress amplitude) is observed for all test temperatures and loading conditions. A large amount of softening from the first cycle onwards occurs, after which a gradual change in the stress values under all test conditions is detected. Three stages can be distinguished in the stress amplitude plots. The first stage is characterized by a gradual decrease in both tensile and compressive peak stress (due to inelastic strain). The second stage shows a steady state with a constant rate of the cyclic softening. In the last stage, a significant decrease in the stress amplitude is observed (due to damage localizations and increase in the inelastic strain). The amount of softening and the softening rates are accelerated at higher test temperatures, while the hold has a slight impact on this behaviour. Moreover, experimental findings also indicate a gradual decrease of the deformation energy density during the fatigue process. The hysteresis area evolution reveals that the deformation energy density decreases with increasing number of cycles, and this decrease is found more pronounced for high test temperatures as shown in Figure 5(b).

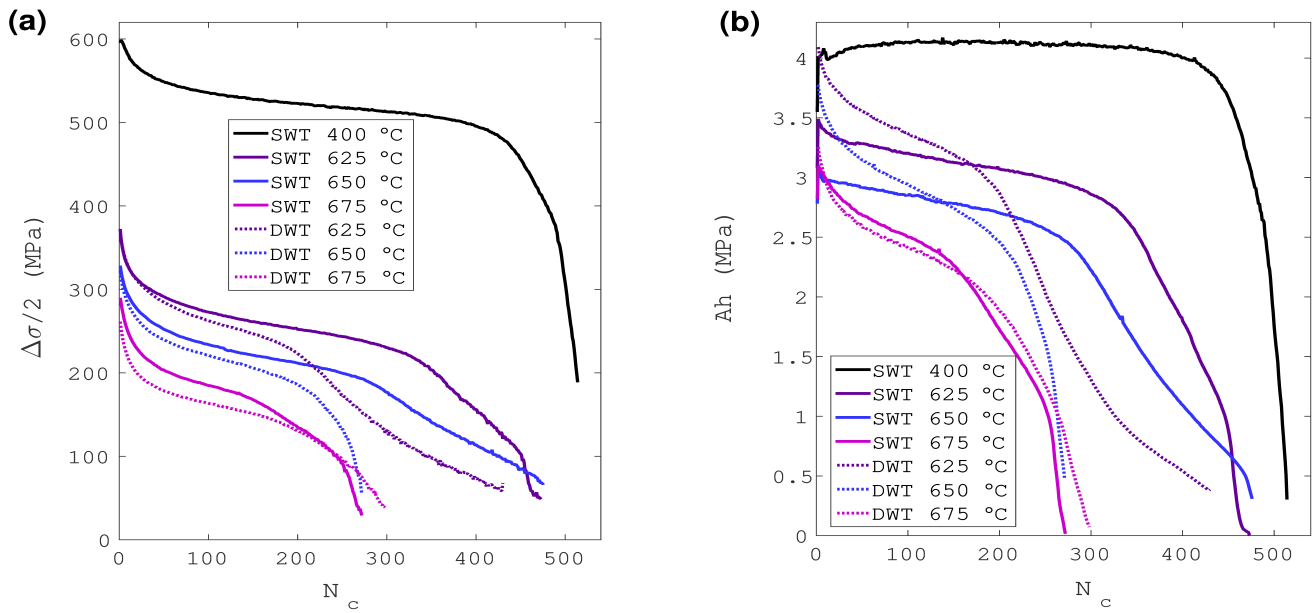

Figure 5: A comparative plot of hysteresis variations for both SWT and DWT at the selected temperatures, highlighted by (a) the stress amplitude evolution, $\Delta\sigma/2$, and (b) the hysteresis area blackuction, A_h.

3.1.4. Anhysteretic behaviour

Anhysteretic tests with path symmetry during the unloading have been conducted to investigate the long-term viscous effects (below and above the yield) and also to reach and reveal the

equilibrium stress response of the material at different strain levels. The reason of conducting such experimental investigation is motivated by the fact that some conventional power plant components are exposed to elevated temperature conditions that activate significant amounts of creep (long term viscous effects) for stress much lower than any reasonable interpretation of yield (Cortellino et al., 2017). So, it is of great interest to characterize the material behaviour below the yield and see if it remains elastic. Indeed, in many practical implementations of High-Cr steels, stress magnitudes are consideblack in the elastic regime and viscous effects are entirely attributed to viscoplastic mechanisms where viscous strain accumulation is only possible at stresses greater than the yield. This experimental investigation by conducting such advanced tests attempts to demonstrate the importance of incorporating viscoelastic effects (even below the yield) in the commonly implemented elasto-viscoplastic constitutive Chaboche type models (Chaboche, 2008).

The cyclic anhysteretic tests presented hereafter include several relaxation plateaus with strain levels that allow to work below and above the yield stress. Figure 6 shows the anhysteretic responses at the selected test temperatures studied over a large range of imposed strains. Several conclusions can be pointed out from the results:

- At the first relaxation step, the material exhibits a highly temperature dependent viscous behaviour. In Figure 6(d), the stress relaxes to approximately 98MPa for 625°C, 78MPa for 650°C and 75MPa for 675°C, values which are below that of the yield stress of the MarBN steel (circa 130MPa for 625°C, 102MPa for 650°C and 94MPa for 675°C).

- The viscous effects occur on a long-time scale. Although strain levels are increasing, the relaxation stress amplitudes at the last relaxation steps are similar, Figure 6(b-c).

- The anhysteretic loops become contracted and shrank at the second anhysteretic block with a same hardening behaviour as that observed within the previous sawtooth cycles, Figure 6(e-f).

- During the unloading, the relaxed stress amplitude is almost the same for all applied temperatures; this observation is not valid at compressive region where the relaxed stress

variations show a highly temperature dependent response.

- The cyclic response of the investigated material shows irrecoverable strains below and above what is consideblack as the yield stress of the MarBN steel. It is however difficult to conclude whether residual strains stem from (visco-) plastic flow or from very long-term recoverable viscosity.

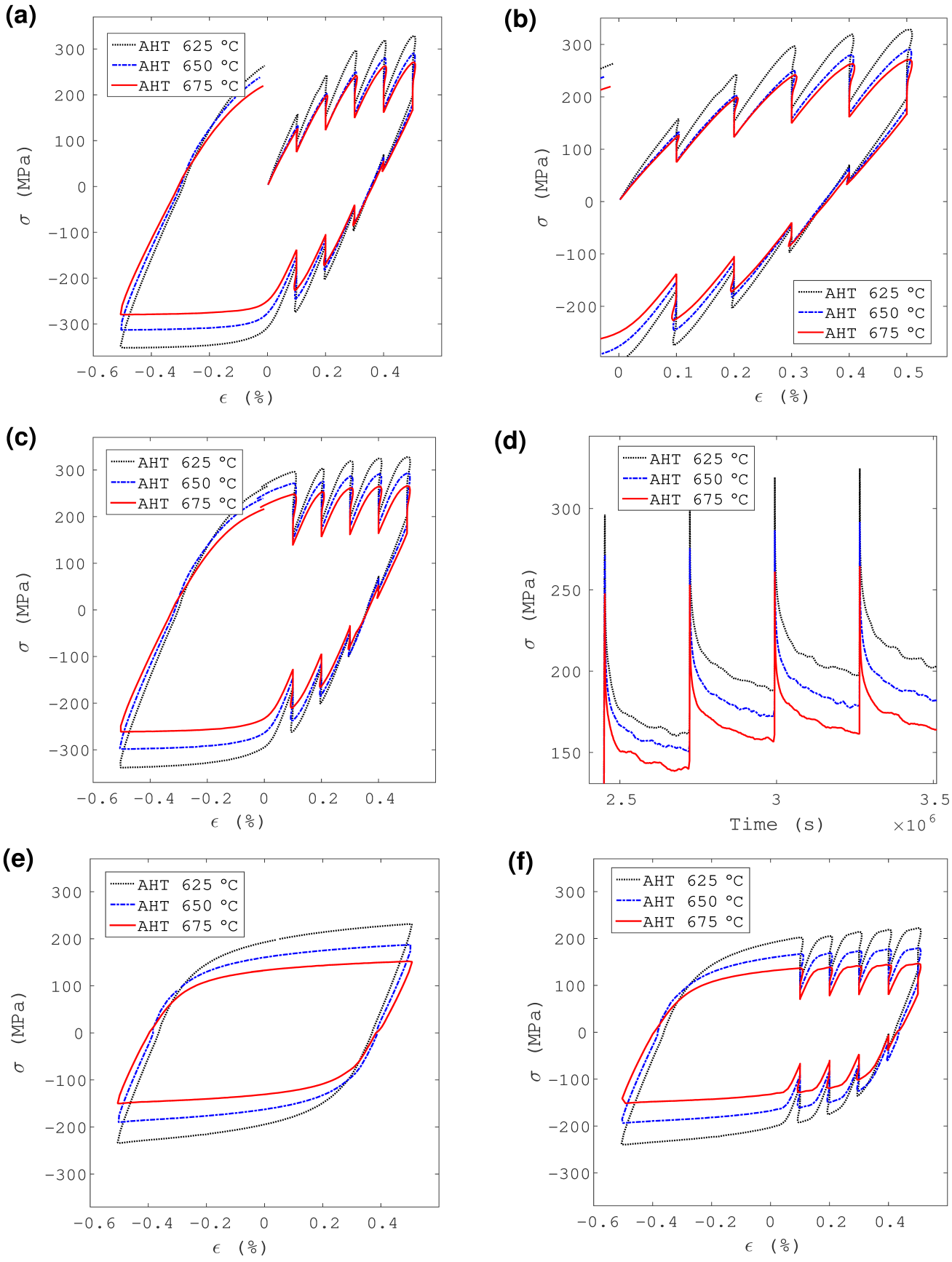

Figure 6: Anhysteretic responses of the MarBN steel at the selected temperatures. Figures are arranged to show (a-b) material response at the first anhysteretic cycle, (c) material response at the second anhysteretic cycle, (d) relaxation response at the ongoing tensile region of the second anhysteretic cycle, (e) material response during the last sawtooth test of the first block and (f) anhysteretic response of the first cycle of the second block.

3.1.5. *Cyclic creep-recovery behaviour*

Cyclic creep-recovery tests, CRT, have been performed to deeply investigate the long-term viscosity effects at several stress levels. These tests are designed to distinguish between long-term viscoelastic and viscoplastic mechanisms. Figure 7(a) shows the axial strain versus time plots of the MarBN steel extracted from CRT conducted under different stress levels for the 625°C test temperature. The corresponding mechanical response is given in Figure 7(b). It can be noted from the plots that at low stress levels, time-dependent effects are pronounced with inelastic strain partially recoveblack (around 0.05%). At higher stress levels, large amounts of irrecoverable strain appear which are consideblack to be consequence of a significant viscoplastic flow. These residual strains seem to accumulate cycle after cycle with values of 0.42% at 210% of the yield strength. Finally, the ratcheting behaviour is observed in Figure 7(b) highlighted by the shifting of the hysteresis loops.

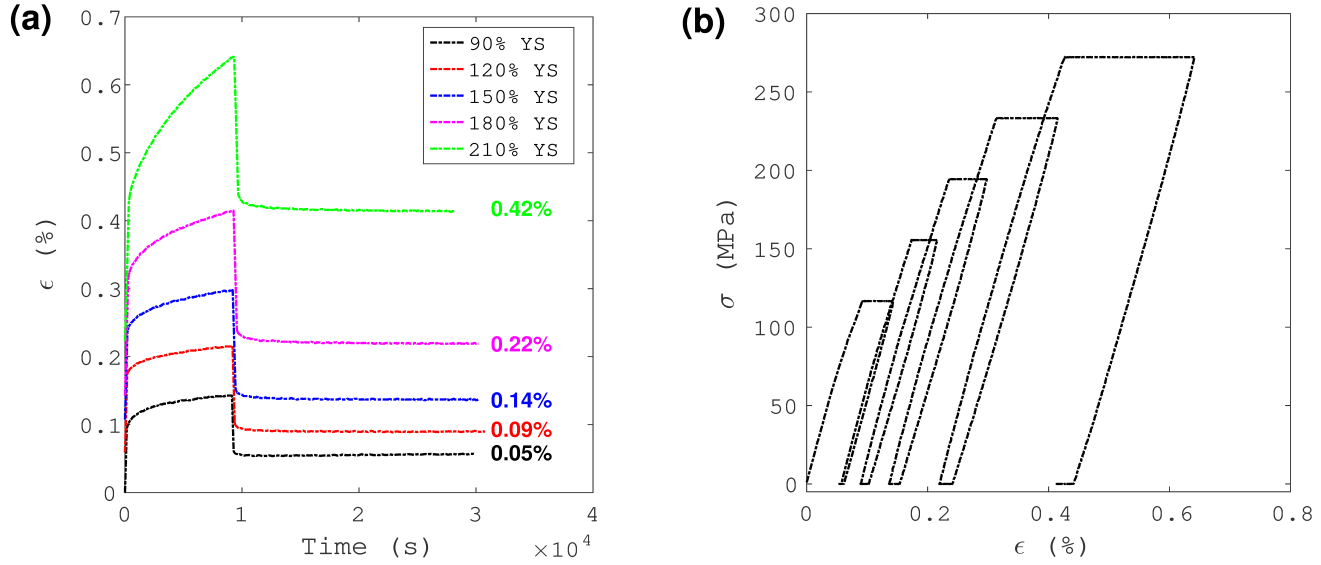

Figure 7: Cyclic creep-recovery tests for the 625°C test temperature conducted at several stress levels until failure: (a) the axial strain versus time plot highlighting the un-recoveblack strain stoblack within the material; (b) the associated mechanical response showing the cyclic ratcheting effect.

3.2. *Material characterisation*

Ruptublack specimens were examined in detail after SWT, DWT and CRT to investigate the variation in deformation and rupture behaviour upon different testing conditions. Fractography examination was conducted on the fracture surfaces of specimens, followed by detailed

metallographic examination using EBSD and micro-hardness mapping.

3.2.1. *Fractography Examination*

Topography of the samples' fracture surfaces was examined using SE imaging on the specimens experiencing SWT, DWT and CRT at 625°C, Figure 8.

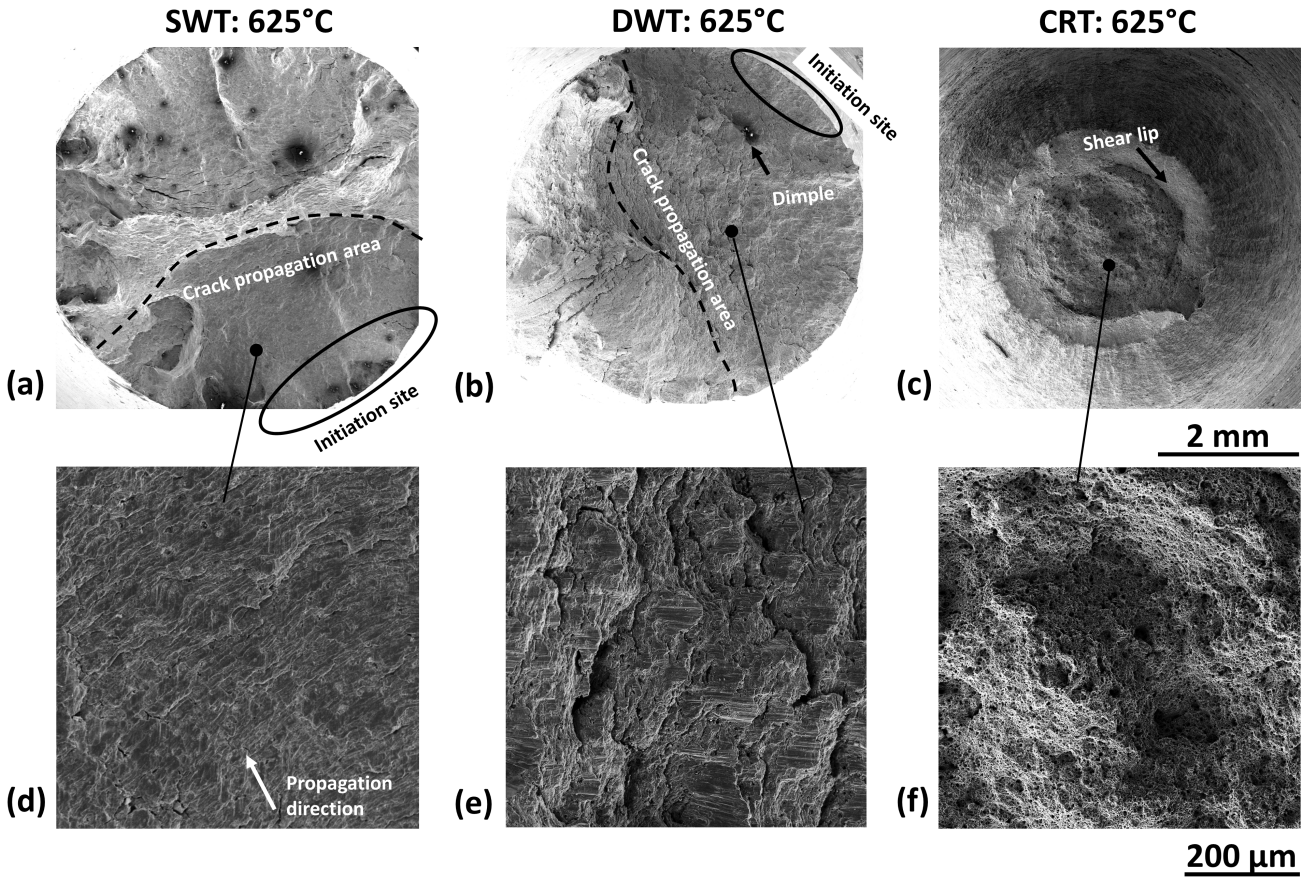

Figure 8: Topography of fracture surface after (a and d) SWT, (b and e) DWT and (c and f) CRT at 625°C.

Figure 8(a and d) demonstrate that the specimen experiencing SWT at 625°C was ruptublack as a result of fatigue crack propagation. The major crack was initiated from the outer surface of the specimen, followed by rapid crack propagation (contoublack by dashed lines) as marked by fatigue striations aligned perpendicular to the propagation direction. The regions of crack initiation are small in area and not distinctively differentiated from the area of crack propagation due to rapid crack propagation. The specimen experiencing DWT at 625°C (Figure 8b) was ruptublack in a similar manner as compablack to the specimen experiencing SWT. This is evidenced by the presence of striations and dimples on fracture surface, Figure 8(b and e)). A

larger interspacing distance between striations was observed after DWT testing as a result of holding period in each loading cycle. The transgranular fracture surface observed after DWT is consistent with the previous observations from similar 9-12% Cr martensitic steels upon stress/strain-controlled dwell fatigue testing conducted at similar conditions (Fournier et al., 2008). The transition in rupture behaviour between SWT and DWT specimens suggests that the hold duration during DWT imposes a dominating effect over the influence of cyclic loading on the manner of rupture. The specimen experiencing CRT was ruptublack in a ductile manner as evidenced by a dimpled surface, Figure 8(c and f). The dimpled topography of fracture surface has been previously observed after tensile testing (Mishnev et al., 2016) and short-term creep testing (Benaarbia et al., 2018b) conducted in the high temperature regime as a result of plasticity instability. The rupture of CRT specimen was therefore consideblack to take place in a transgranular manner via the coalescence of plasticity induced micro-voids during the hold duration at a stress level above the yield strength (Lin et al., 2005).

3.2.2. EBSD mapping analysis

EBSD mapping analysis was conducted in the longitudinal cross-section in the as-received state and after SWT, DWT and CRT at 625°C in the regions close to the fracture surface, Figure 9. The EBSD maps were collected adjacent to the crack propagation area and the dimpled region as demonstrated in Figure 9 in the SWT/DWT and CRT specimens, respectively.

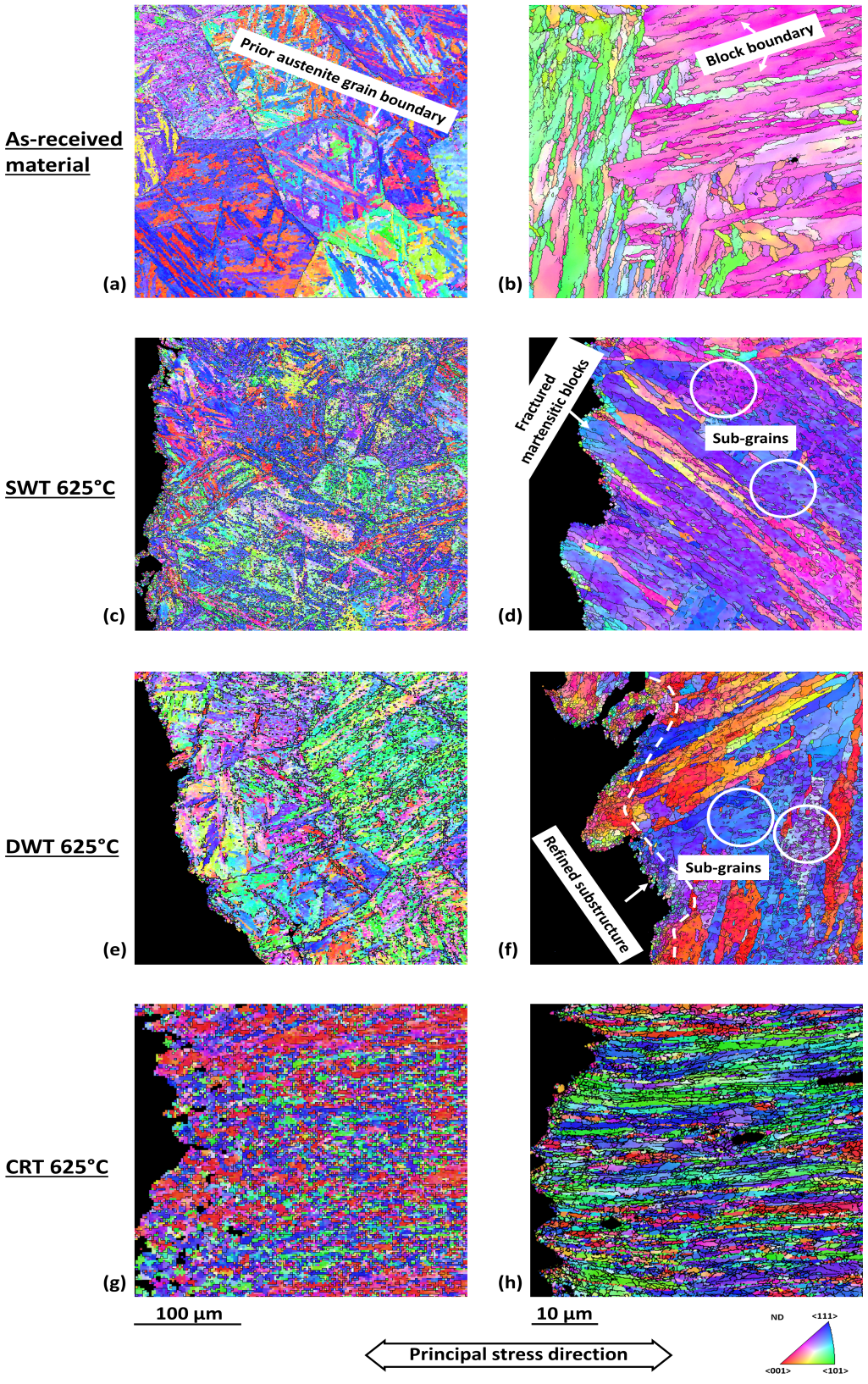

Figure 9: EBSD maps showing (a and b) the initial microstructure in the as-received state and the microstructure in the regions adjacent to the fracture surfaces after (c and d) SWT, (e and f) DWT and (g and h) CRT at 625°C. Typical regions demonstrating a refined grain structure are indicated by white circles in (d) and (f).

The initial microstructure in the as-received state is composed of Prior Austenite Grains (PAGs) that are > 200 µm in diameter (Figure 9(a)) and elongated martensitic blocks with a width between 2 and 5 µm, Figure 9(b). Figure 9(c and e) demonstrate that the original PAG structure was not significantly changed during SWT and DWT, whereas the formation of sub-grains that are < 1 µm in diameter was extensively observed within the martensitic blocks, Figure 9(d and f). This is consistent with existing observations from similar 9-12% Cr steels demonstrating similar resultant microstructures after LCF exposure (Mishnev et al., 2016; Verma et al., 2016). The extensive formation of sub-grains within the martensitic substructure was attributed to the transformation from an unstable martensitic lath structure to a cellular substructure via the rearrangement of pre-existing dislocations at the elevated temperatures (Mishnev et al., 2016). The formation of sub- grains is therefore consideblack to result in a decrease in dislocation density and cause cyclic softening as observed in Figure 5.

In addition, significant structural refinement has been observed in the region < 5 µm from the fracture surface in the DWT specimen (Figure 9(f)), whereas the refinement of the martensitic substructure was not evident in the SWT specimen. The presence of structural refinement in martensitic steels has been previously reported as a consequence of significant plastic deformation at a high strain rate (Huang et al., 2012; Zhang et al., 2015). This further suggests that the deformation and rupture of the specimen experiencing DWT is involved with plasticity related mechanisms.

The specimen experiencing CRT demonstrates a significantly refined microstructure in the region close to the fracture surface, Figure 9(g and h). The original PAG structure and the martensitic substructure were both refined to an equiaxed morphology, with the vicinities corresponding to the original martensitic blocks distorted along the principal stress direction, Figure 9(h). The significant refinement of the original martensitic microstructure has been observed from similar materials upon rapid plastic deformation at elevated temperature (Huang et al., 2012; Zhang et al., 2015; Benaarbia et al., 2018b). The CRT specimen was therefore consideblack to experience significant plastic deformation prior to rupture.

3.2.3. Hardness mapping

Hardness measurement was firstly performed in the as-received MarBN steel prior to LCF testing at a loading weight of 10 kg and 0.2 kg. The values of hardness obtained from the as-received material are measuring 249±2 HV10 and 261±8 HV0.2 at different testing conditions. Hardness measurement was further conducted close to the boundary between gauge and head portions of SWT and DWT specimens at a loading weight of 10 kg. The hardness values obtained from the specimens experiencing SWT and DWT at 625°C are 271±3 and 260±8 HV10, respectively. The variation of hardness in the region close to fracture surface was further characterised using hardness mapping analysis at a loading weight of 0.2 kg after SWT and DWT at 625°C, Figure 10.

Figure 10(a) demonstrates that hardness varies between 198 and 229 HV0.2 in the region < 4 mm away from fracture surface in the specimen experiencing SWT at 625°C. The hardness in the regions closer to the head portion (i.e. > 4 mm from fracture surface) is higher and in the range between 242 and 291 HV0.2 in the same specimen, Figure 10(a). The variation of hardness is not evident without a clear trend in the specimen experiencing DWT, Figure 10(b). Hardness varies between 218 and 247 HV0.2 in the gauge portion of the specimen experiencing DWT. The hardness values measublack from the gauge portion are considerably lower than the values measublack from the as-received material (i.e. 261±8 HV0.2). The lower hardness in the gauge regions close to the fracture surface has further confirmed the deterioration of matrix properties upon LCF exposure at both the SWT and DWT conditions. The transformation of martensitic substructure and the decrease of dislocation density accompanied by the formation of sub-grains may cause a decrease in the hardness and the stress amplitude measublack from cyclic fatigue testing, Figure 10. The value of hardness as measublack from the region close to the fracture surface of the CRT specimen is evidently higher than the region further away. This can be attributed to a higher volume density of dislocations in the region close to the fracture surface upon the occurrence of necking due to localised plasticity instability (Benaarbia et al., 2018b). This is further evidenced by the observation of significantly distorted and refined martensitic microstructure as shown in Figure 9.

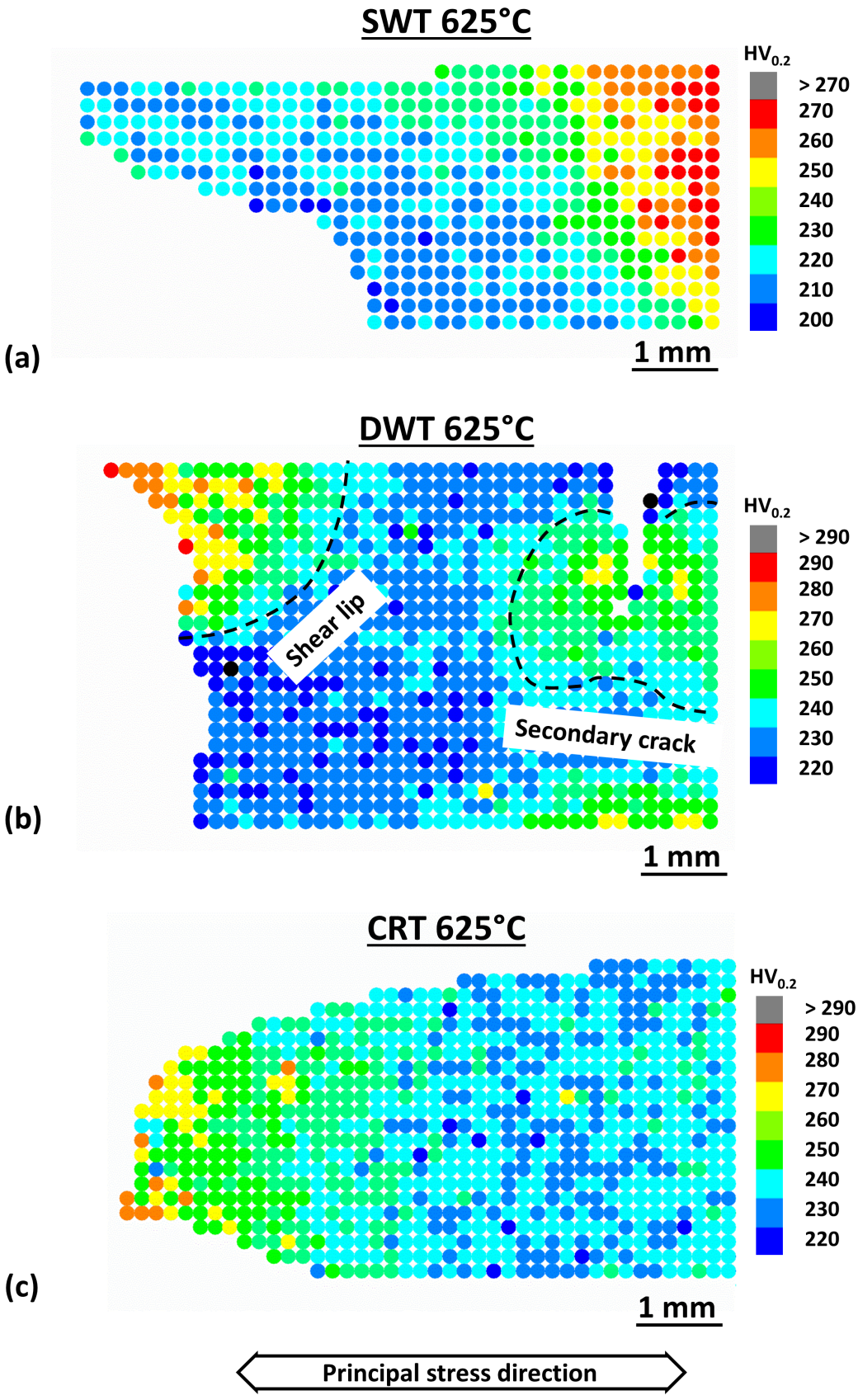

Figure 10: Hardness maps collected from the regions close to fracture surfaces in the specimens experiencing (a) SWT, (b) DWT and (c) CRT at 625°C.

4. Conclusions and future work

Extensive experimental work has been conducted to investigate the high temperature low cycle fatigue behaviour of MarBN steel at bulk and micro-scales. Fully-reversed tests with zero- and hold-tensile periods, anhysteretic tests with hold- tensile periods at ascending strain levels, and cyclic creep-recovery tests at different stress ranges, were conducted. The mechanical investigations were combined with microstructural analyses (through SEM, EBSD and hardness mapping) to further emphasize the leading deformation mechanisms. The main conclusions are listed below:

- A continuous accelerated cyclic softening and a decelerated stress relaxation behaviour were observed for all test temperatures. The first was attributed to the accumulated inelastic transformation from the creep mechanism during the dwell period at the peak tensile strain of the fatigue cycle, while the second was ascribed to the blackuction in the viscous stress due to the continuous cyclic softening.

- Large amounts of irrecoverable strains below and above the yield were highlighted through AHT, while the viscous effects were found to occur on a long time-scale. The irreversible strains were attributed to either viscoplastic and/or long-term viscous effects.

- Time-dependent effects at low stress levels were pronounced with inelastic strain partially recoveblack (see the cyclic creep-recovery tests). At higher stress levels large amounts of irrecoverable strains appeablack.

- Specimens experiencing SWT were ruptublack as a result of fatigue crack propagation. The rupture for specimens experiencing DWT and CRT was consideblack to take place in a transgranular and ductile manner (evidenced by a dimpled surface) via the coalescence of plasticity induced micro-voids during the hold duration.

- An extensive formation of sub-grains within the martensitic substructure was observed for all test conditions. This was further related with a decrease in dislocation density that causes cyclic softening. A significant structural refinement for the martensitic substructure

was also observed for both DWT and CRT conditions. This refinement was attributed to the plastic deformation.

- Same hardness variations for both SWT and DWT conditions were reported. The decrease in hardness values was essentially due to the transformation in martensitic substructure.

Based on the conclusions drawn above, future work will focus on the modelling of the viscoplastic behaviour of the MarBN steel at high temperature conditions. This should be undertaken focusing on the incorporation of microstructural features in the model constitutive equations. The inclusion of such microstructural information will undoubtedly enhance the fundamental understanding that the model can provide. Models based on dislocation density should have an enhanced physical meaning. Dislocation densities can thus be incorporated as internal state variables, and their evolution can be modelled based on the storage and annihilation processes for dislocations.

5. Acknowledgments

This work is supported by the Engineering and Physical Sciences Research Council (grant numbers: EP/N509991/1 and EP/N509942/1).

The authors gratefully acknowledge the following partners for their valuable contributions: Doosan Babcock, GE Power, Uniper Technologies, Metrode Products, Goodwin Steel Castings and Wyman-Gordon. Specific acknowledgments to GE Power for providing the test material and to Mr. Shane Maskill (University of Nottingham) for his support in the experimental testing.

References

References

Abe, F., Tabuchi, M., Semba, H., Igarashi, M., Yoshizawa, M., Komar, N., Fujita, A., 2008. Feasibility of marbn steel for application to thick section boiler components in usc power plant at 650°c. 5th International Conference on Advances in Materials Technology for Fossil Power Plants, Marco Island, FL, Oct. 3-5 , 92–106.

Bassi, F., Foletti, S., Conte, A.L., 2015. Creep fatigue crack growth and fracture mechanisms of t/p91 power plant steel. Materials at High Temperatures 32, 250–255.

Batista, M., Marinelli, M., Herenu, S., Alvarez-Armas, I., 2015. The role of microstructure in fatigue crack initiation of 9-12%cr reduced activation ferritic-martensitic steel. International Journal of Fatigue 72, 75 – 79.

Benaarbia, A., Rouse, J., Sun, W., 2018a. A thermodynamically-based viscoelastic-viscoplastic model for the high temperature cyclic behaviour of 9–12% cr steels. International Journal of Plasticity 107, 100 – 121.

Benaarbia, A., Xu, X., Sun, W., Becker, A., Jepson, M.A., 2018b. Investigation of short-term creep deformation mechanisms in marbn steel at elevated temperatures. Materials Science and Engineering: A 734, 491 – 505.

Chaboche, J., 2008. A review of some plasticity and viscoplasticity constitutive theories. International Journal of Plasticity 24, 1642 – 1693. Special Issue in Honor of Jean-Louis Chaboche.

Chen, R., Armaki, H.G., Maruyama, K., Igarashi, M., 2011. Long-term microstructural degradation and creep strength in gr.91 steel. Materials Science and Engineering: A 528, 4390 – 4394.

Cortellino, F., Rouse, J.P., Cacciapuoti, B., Sun, W., Hyde, T.H., 2017. Experimental and numerical analysis of initial plasticity in p91 steel small punch creep samples. Experimental Mechanics 57, 1193 – 1212.

Fournier, B., Dalle, F., Sauzay, M., Longour, J., Salvi, M., Caës, C., Tournié, I., Giroux, P.F., Kim, S.H., 2011. Comparison of various 9–12%cr steels under fatigue and creep-fatigue loadings at high temperature. Materials Science and Engineering: A 528, 6934 – 6945.

Fournier, B., Sauzay, M., Caës, C., Noblecourt, M., Mottot, M., Bougault, A., Rabeau, V., Pineau, A., 2008. Creep-fatigue-oxidation interactions in a 9cr-1mo martensitic steel. part i: Effect of tensile holding period on fatigue lifetime. International Journal of Fatigue 30, 649 – 662.

Gianfrancesco, D., 2017. Materials for ultra-supercritical and advanced ultra- supercritical power plants. Woodhead Publishing , 1–49.

Guguloth, K., Sivaprasad, S., Chakrabarti, D., Tarafder, S., 2014. Low-cyclic fatigue behavior of modified 9cr-1mo steel at elevated temperature. Materials Science and Engineering: A 604, 196 – 206.

Huang, X., Morito, S., Hansen, N., Maki, T., 2012. Ultrafine structure and high strength in cold-rolled martensite. Metallurgical and Materials Transactions A 43, 3517–3531.

Lin, J., Liu, Y., Dean, T.A., 2005. A review on damage mechanisms, models and calibration methods under various deformation conditions. International Journal of Damage Mechanics 14, 299–319.

Mannan, S., Valsan, M., 2006. High-temperature low cycle fatigue, creep-fatigue and thermo-mechanical fatigue of steels and their welds. International Journal of Mechanical Sciences 48, 160 – 175. 7th Asia-Pacific Symposium on Advances in Engineering Plasticity and its Applications (AEPA 2004).

Mishnev, R., Dudova, N., Kaibyshev, R., 2016. Low cycle fatigue behavior of a 10cr-2w-mo-3co-nbv steel. International Journal of Fatigue 83, 344 – 355.

Pineau, A., 2014. High temperature fatigue - a comprehensive review. Creep fatigue crack development symposium .

Pineau, A., Antolovich, S.D., 2015. High temperature fatigue: behaviour of three typical classes of structural materials. Materials at High Temperatures 32, 298–317.

Rae, Y., Benaarbia, A., Hughes, J., Sun, W., 2019. Experimental characterisation and computational modelling of cyclic viscoplastic behaviour of turbine steel. International Journal of Fatigue 124, 581 – 594.

Saad, A., Hyde, T., Sun, W., Hyde, C., Tanner, D., 2013. Characterization of viscoplasticity

behaviour of p91 and p92 power plant steels. International Journal of Pressure Vessels and Piping 111-112, 246 – 252.

Shankar, V., Bauer, V., Sandhya, R., Mathew, M., Christ, H.J., 2012. Low cycle fatigue and thermo-mechanical fatigue behavior of modified 9cr-1mo ferritic steel at elevated temperatures. Journal of Nuclear Materials 420, 23 – 30.

Shankar, V., Valsan, M., Rao, K.B.S., Kannan, R., Mannan, S., Pathak, S., 2006. Low cycle fatigue behavior and microstructural evolution of modified 9cr-1mo ferritic steel. Materials Science and Engineering: A 437, 413 – 422.

Swindeman, R., Santella, M., Maziasz, P., Roberts, B., Coleman, K., 2004. Issues in replacing cr-mo steels and stainless steels with 9cr-1mo-v steel. International Journal of Pressure Vessels and Piping 81, 507 – 512. The 7th International Conference on Operating Pressure Equipment.

Verma, P., Srinivas, N.S., Singh, S., Singh, V., 2016. Low cycle fatigue behavior of modified 9cr-1mo steel at room temperature. Materials Science and Engineering: A 652, 30 – 41.

Viswanathan, R., Henry, J.F., Tanzosh, J., Stanko, G., Shingledecker, J., Vitalis, B., Purgert, R., 2005. U.s. program on materials technology for ultra-supercritical coal power plants. Journal of Materials Engineering and Performance 14, 281–292.

Wang, X., Zhang, W., Gong, J., Wahab, M.A., 2018. Low cycle fatigue and creep fatigue interaction behavior of 9cr-0.5mo-1.8w-v-nb heat-resistant steel at high temperature. Journal of Nuclear Materials 505, 73 – 84.

Yan, W., Wang, W., Shan, Y.Y., Yang, K., 2013. Microstructural stability of 9-12%cr ferrite/martensite heat-resistant steels. Frontiers of Materials Science 7, 1–27.

Zhang, S.L., Xuan, F.Z., 2017. Interaction of cyclic softening and stress relaxation of 9–12% cr steel under strain-controlled fatigue-creep condition: Experimental and modeling. International Journal of Plasticity 98, 45 – 64.

Zhang, S.L., Xuan, F.Z., Guo, S.J., Zhao, P., 2017. The role of anelastic recovery in the creep-fatigue interaction of 9–12% cr steel at high temperature. International Journal of Mechanical Sciences 122, 95 – 103.

Zhang, Z., Mishin, O., Tao, N., Pantleon, W., 2015. Microstructure and annealing behavior of a modified 9cr-1mo steel after dynamic plastic deformation to different strains. Journal of Nuclear Materials 458, 64 – 69.

Zhu, X., Chen, H., Xuan, F., Chen, X., 2019. On the creep fatigue and creep rupture behaviours of 9–12% cr steam turbine rotor. European Journal of Mechanics - A/Solids 76, 263 – 278.